GDCh

Communications

Angewandte
Chemie
International Edition
www.angewandte.org

Carbon Nanotubes | Hot Paper

Single-Walled Carbon Nanotubes Encapsulated within Metallacycles

Alejandro López-Moreno, Susana Ibáñez, Sara Moreno-Da Silva, Luisa Ruiz-González, Natalia Martín Sabanés, Eduardo Peris,* and Emilio M. Pérez*

Dedicated to Professor Sir J. Fraser Stoddart on the occasion of his 80th birthday

Abstract: Mechanically interlocked derivatives of carbon nanotubes (MINTs) are interesting nanotube products since they show high stability without altering the carbon nanotube structure. So far, MINTs have been synthesized using ring-closing metathesis, disulfide exchange reaction, H-bonding or direct threading with macrocycles. Here, we describe the encapsulation of single-walled carbon nanotubes within a palladium-based metallosquare. The formation of MINTs was confirmed by a variety of techniques, including high-resolution transmission electron microscopy. We find the making of these MINTs is remarkably sensitive to structural variations of the metallo-assemblies. When a metallosquare with a cavity of appropriate shape and size is used, the formation of the MINT proceeds successfully by both templated clipping and direct threading. Our studies also show indications on how supramolecular coordination complexes can help expand the potential applications of MINTs.

Chemical modification of single-walled carbon nanotubes (SWNTs)[1] is a critical step to exploit their properties.[2] To name just two recent prominent examples, the covalent modification of the SWNTs can be used to change their surface properties and enhance their performance as optical sensors in biologically relevant environments.[3] In 2019, a series of cleverly designed processes based on the non-covalent functionalization of SWNTs (pretreatment with hexamethyldisilazane and bis(trimethylsilyl)amine to promote adhesion to a silicon wafer, adhesion coating with polymethylglutarimide, and mechanical exfoliation), were key in the fabrication of the first functioning modern microprocessor based on carbon nanotube field-effect transistors.[4] In 2014, some of us described a clipping strategy to synthesize mechanically interlocked derivatives of SWNTs (MINTs), which can be viewed as rotaxane-like species in which the SWNTs act as threads.[5] In our original method, the nanotube was first trapped supramolecularly within the two recognition motifs of a U-shaped molecule featuring two terminal alkenes, which were subsequently coupled via a ring-closing metathesis (RCM) producing the annulation of the molecule around the SWNT.[6] Thanks to the mechanical link, the resulting MINTs show similar stability as covalently-modified carbon nanotubes but preserving its structure.[7]

Since these initial works, we found that this method can be extended to numerous types of recognition motifs for SWNTs.[8] We also provided evidence that the formation of MINTs shows promise in various applications, such as for reinforcing polymers,[9] and for designing metal-free catalysts[10] or qubits.[11] In the last years, several groups described different strategies towards the synthesis of MINTs, such as the reversible formation of macrocycles through disulfide bonds,[12] hydrogen bond self-assembled macrocycles,[13] or the direct threading through rigid macrocycles.[14]

Although the chemistry of MINTs experienced a significant development in the last few years, we are unaware of examples of MINTs made by the threading of SWNTs through the cavity of supramolecular coordination complexes (SCCs).[15] Compared to MINTs built with purely organic supramolecular assemblies, SCCs may introduce a new dimension in the resulting MINT, as the presence of the metal can provide enhanced photoelectrochemical properties that can help expanding their applications. During the past few years, some of us described a series of N-heterocyclic-carbene (NHC) based supramolecular organometallic complexes (SOCs), which were used as hosts for encapsulating a variety of organic and inorganic guests.[16] In particular, we found that some of our Ni-[17] and Pd-containing[18] metallosupramolecular assemblies based on a pyrene-bis-imidazolylidene ligand (**1** and **2** in Figure 1a),

[*] Dr. A. López-Moreno, S. Moreno-Da Silva, Dr. N. M. Sabanés, Prof. E. M. Pérez
IMDEA Nanociencia
C/Faraday 9, 28049 Madrid (Spain)
E-mail: emilio.perez@imdea.org

Dr. S. Ibáñez, Prof. E. Peris
Institute of Advanced Materials (INAM), Centro de Innovación en Química Avanzada (ORFEO-CINQA), Universitat Jaume I
Av. Vicente Sos Baynat s/n.,12071 Castellón (Spain)
E-mail: eperis@uji.es

Dr. L. Ruiz-González
Departamento de Química Inorgánica y Centro Nacional de Microscopía Electrónica, Universidad Complutense de Madrid
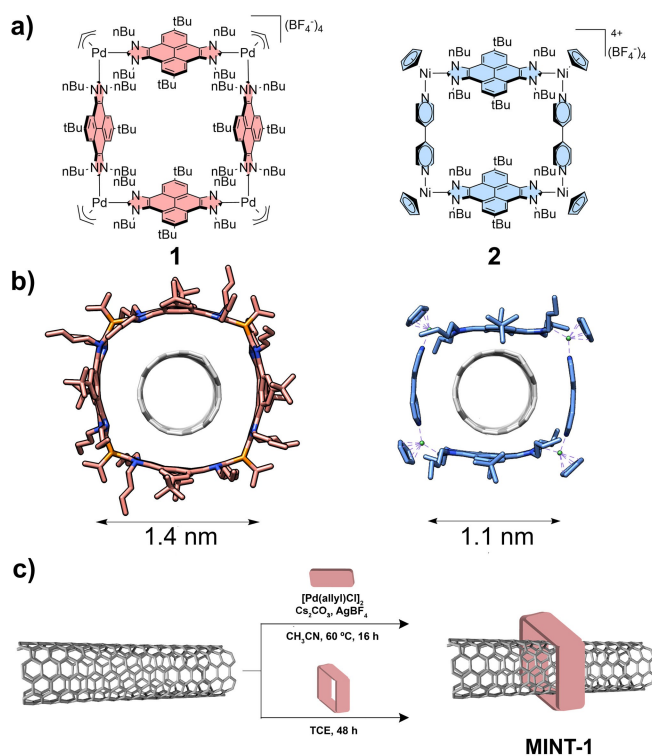28040 Madrid (Spain)

Figure 1. a) Chemical structure of metallosquare **1** and **2**. b) Energy-minimized (UFF) model of MINT-**1** and MINT-**2**. c) Schematic representation of MINT-**1** through two different routes.

were able to adapt their shapes to the size of the encapsulated fullerenes (C_{60} or C_{70}). This guest-induced fitting effect was manifested by the compression or the expansion of the metallacycles, and by the bending of the pyrene moieties of the bis-NHC ligand for maximizing the face-to-face overlap with the convex surface of the fullerenes. We thought that the high binding affinities of our metallo-assemblies to fullerenes, together with their great shape adaptability, could make these hosts perfect candidates for the mechanical interlocking of SWNTs and give access to a new class of transition metal-doped MINTs.

Considering all the above, herein we describe the preparation of metallacycle-containing MINTs, which can be performed by templated self-assembly of the molecular components around the SWNTs, or by direct encapsulation of the nanotube in the cavity of the preformed metallacycle (Figure 1c).

To attempt the preparation of MINTs we chose a collection of building blocks that would lead to macrocycles **1** or **2** (Figure 1a). The metallosquare **1** is bound by four pyrene-bis-imidazolylidene ligands that confer its structure with a great level of stability, due to the strong NHC–Pd bonds. In addition, this structure can be regarded as 'static', in the sense that it does not reversibly assemble and dissemble. The nickel-conjoined metallacycle **2** is more dynamic, as the two more labile bipyridine ligands can reversibly dissociate, but it shows a slightly smaller cavity (Figure 1b). As described above, both **1** and **2** can associate

fullerenes C_{60} and C_{70}, which are equivalent in size to the diameter of the (6,5)-SWNTs used in this work.

The templated preparation of MINT-**1** was performed as follows. To a suspension of (6,5)-SWNTs in anhydrous acetonitrile were added the pyrene-bis(imidazolium) salt, [Pd(allyl)Cl]$_2$, AgBF$_4$ and Cs$_2$CO$_3$ (see Supporting Information for full details), and the suspension was allowed to react for 16 h at 60 °C. The resulting MINT-**1** was recovered by filtration through a polytetrafluoroethylene (PTFE) membrane with a pore size of 0.2 μm and washed with CH$_3$CN and CH$_2$Cl$_2$ to remove all non-interlocked materials. After purification, the samples were subjected to thermogravimetric analysis (TGA) in order to quantify the degree of functionalization. In three separate experiments, MINT-**1** showed weight losses of 26–28%, which correspond to a reasonable degree of functionalization for MINTs.[7] We also carried out control experiments in which we mixed the pyrene-bis(imidazolium) salt with (6,5)-SWNTs without Cs$_2$CO$_3$, under otherwise identical conditions to the MINT-forming reaction. These samples showed less than 5% functionalization after the washing step. Likewise, when the reaction was performed in absence of [Pd(allyl)Cl]$_2$ under the same conditions, (6,5)-SWNTs were also recovered without physisorbed products on the SWNTs. Finally, a control experiment with preformed metallosquare-**1** (0.0014 mmol) in a suspension of 10 mg of (6,5)-SWNTs in 10 mL of anhydrous acetonitrile resulted in a lower but significant functionalization of 13%. Considering these results, we optimized the preparation of MINTs by direct encapsulation within **1** taking inspiration from the results of Ohe et al.[15] Preformed metallosquare **1** was added to a dispersion of (6,5)-SWNTs in 1,1′,2,2′-tetrachloroethane (TCE), and the mixture was stirred at room temperature for 48 h. After this time MINT-**1** was recovered by filtration and washed profusely. The sample was analyzed by TGA showing 29% of functionalization and proving that both methods are effective and comparable (Figure S1). We previously reported that MINTs show remarkable stability, comparable to that of covalently modified nanotubes while maintaining the native covalent structure of the SWNTs.[5–9] To test the stability of functionalization and remove any non-interlocked material that might have survived the initial purification process, we subjected all samples to 30 min of reflux in TCE (bp = 147 °C), followed by a thorough rinse with CH$_3$CN and CH$_2$Cl$_2$. TGA of the resulting samples showed no decrease in the degree of functionalization confirming the high stability of these new MINTs.

To study the structural requirements for the success of the method, and in particular its sensitivity to the size complementarity between the cavity of the macrocycle and the diameter of the SWNT, we investigated the preparation of MINTs with a macrocycle of slightly different size. Reactions were set-up as follows for the attempted formation of MINT-**2**: [NiCpCl]$_2$(pyrene-di-NHC) (1 eq.), 4,4′-bipyridine (1 eq.) and AgBF$_4$ (2 eq.) were added to a suspension of (6,5)-SWNTs in TCE or CH$_2$Cl$_2$ (see Supporting Information for full details). TGA showed very low functionalization (<5%), indicating that the formation of MINT-**2** is negligible, and suggesting that the formation of

the MINT species is extremely sensitive to the fit between macrocycle cavity and SWNT diameter (Figure S2). Similar results have been found for the supramolecular association of fullerenes,[19] and are understood on the basis of a dispersion-dominated interaction, where maximizing van der Waals contacts is essential.[20]

To fully characterize MINT-**1**, we carried out UV/Vis/NIR spectroscopy, photoluminescence excitation intensity mapping (PLE), and Raman spectroscopy, all of which are in agreement with the noncovalent functionalization of the (6,5)-SWNTs with **1**.

In the absorption spectra (D_2O, 1% sodium dodecyl sulphate, 298 K, Figure 2a), the UV region is dominated by the nanotube absorption. The absorption features of **1** (blue in Figure 2a) are distinguishable in the spectrum of MINT-**1** (red in Figure 2a), for the transitions at 268, 302, and 359 nm. The S22 and S11 transitions of the (6,5)-SWNTs are prominent in the vis-NIR, appearing at $\lambda_{max} = 584$ and 1016 nm for the pristine nanotubes (black in Figure 2a). As expected for an intimate metallacycle–SWNT supramolecular interaction, both transitions are shifted hypsochromically to $\lambda_{max} = 578$ and 1001 nm, respectively, upon derivatization to form MINT-**1**. Identical shifts were found for the MINT-**1** sample formed by direct encapsulation (Figure S4). The S22 transition suffers a quantitatively smaller shift due to its higher energy.

Figure 2b contains Raman spectra of the (6,5)-SWNT (black), and MINT-**1** prepared by self-assembly (red) (532 nm excitation, 2 mW). The spectra are an average of 100 individual spectra taken over the sample. Detailed statistical analysis of peak position and intensity ratios are included in Supporting Information section (Figure S3). The spectral features after MINT formation are rather similar to those obtained for (6,5)-SWNT. In particular, radial breathing modes (RBM, 200–400 cm^{-1}), D (ca. 1300 cm^{-1}), G$^-$ (ca. 1535 nm) and G$^+$ (1590 cm^{-1}) modes do not show any relevant shift (see Figure S3), indicating that the electronic structure and the aggregation state of the tubes is mostly preserved upon encapsulation using both methods. Moreover, I_D/I_G ratios, often used to identify structural changes in carbon-based materials due to the increase of defects,[21] is identical within error for (6,5)-SWCNT (0.035 ± 0.009) and MINT-**1** synthesized by self-assembly (0.038 ± 0.009), and remains very low (0.087 ± 0.007) for the MINT-**1** sample synthesized by direct encapsulation. This difference in the I_D/I_G ratio between the different synthetic methods is too small to indicate an increase of covalent defects when using the encapsulation method, and we believe it is better ascribed to differences in the sample preparation method that might lead to, for instance encapsulation of more or less solvent.[22]

The photoluminescence excitation (PLE) map of the (6,5)-SWNTs in the visible-NIR region (Figure 2c) shows an intense peak at $\lambda_{exc} = 565$ nm, $\lambda_{em} = 984$ nm characteristic of the (6,5) chirality, and residual peaks at $\lambda_{exc} = 643$ nm, $\lambda_{em} = 1021$ nm and $\lambda_{exc} = 665$, $\lambda_{em} = 948$ nm, corresponding to (7,5) and (8,3) chiralities. In the MINT-1 sample synthesized by self-assembly (Figure 2d), the luminescence of the (6,5) nanotubes is quenched to approximately 40% and suffers a bathochromic shift to $\lambda_{em} = 984$ nm, compared to a sample of (6,5)-SWNTs with identical optical density. In the MINT-**1** sample synthesized by direct encapsulation (Figure S5b), the luminescence of the (6,5) nanotubes is quenched less efficiently, to approximately 18% and suffers a bathochromic shift to $\lambda_{em} = 993$ nm, compared to the pristine (6,5)-SWNTs. These results might reflect the non-negligible presence of non-interlocked **1** in this sample. With regards to the emission of the pyrene chromophore, in the UV/Vis region, we observe that the fluorescence of metallacycle **1** is blue-shifted from $\lambda_{em} = 403$ nm to $\lambda_{em} = 393$ nm, and quenched by 85%. (Figure S5) upon formation of MINT-**1**.

Finally, the analysis of a sample of MINT-**1** under atomic force microscopy (AFM, dynamic mode) is in clear agreement with the formation of the rotaxane-type species. Figure 3a shows a topographic image of a single SWNT with a height of approximately 1 nm, on which three elevations of approximately 2.5–3 nm are observed (Figure 3a,b). The dimensions and the regularity of these elevations are consistent with the formation of **1** around a SWNT, and rules out the possibility of physisorption of **1** on the SWNT walls.

HR-TEM analysis (200 kV) of samples of MINT-**1** drop casted from a TCE suspension shows mostly bundled nanotubes with heavily functionalized sidewalls, in agreement with the TGA data, although at several instances we can find individualized tubes with objects of adequate size and shape to correspond to macrocycle **1** (see Figures S7 and S8 in the Supporting Information). The chemical composition analysis of these micrographs, as obtained by energy-dispersive spectroscopy, confirms the presence of Pd (see Figure S9). However, under these conditions the organic addends get quickly damaged,[23] and atomic resolution
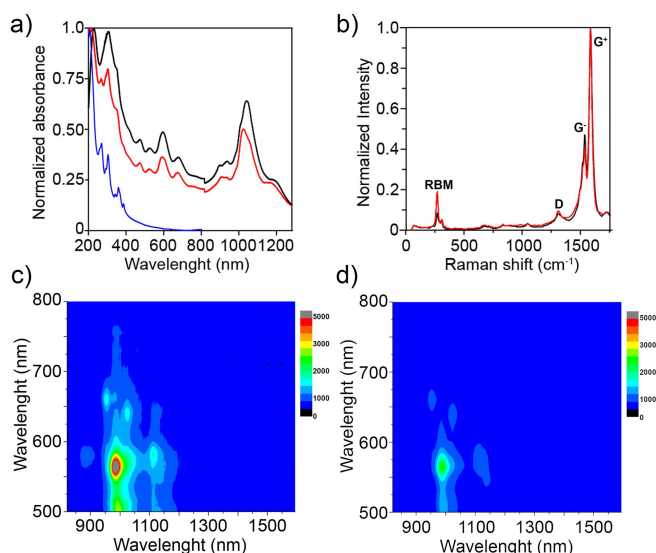

Figure 2. a) UV/Vis/NIR spectra (D_2O, 1% sodium dodecyl sulfate (SDS), 298 K) of pristine (6,5)-SWNTs (black), Metallacycle-**1** (blue), and MINT-**1** (red) prepared by self-assembly. b) Raman spectra ($\lambda_{exc} = 532$ nm) of (6,5)-SWNTs (black), MINT-**1** (red). All spectra are the average of 100 different measurements. PLE intensity maps (D_2O, 1% SDS, 298 K) of c) pristine (6,5)-SWNTs and d) MINT-**1**.
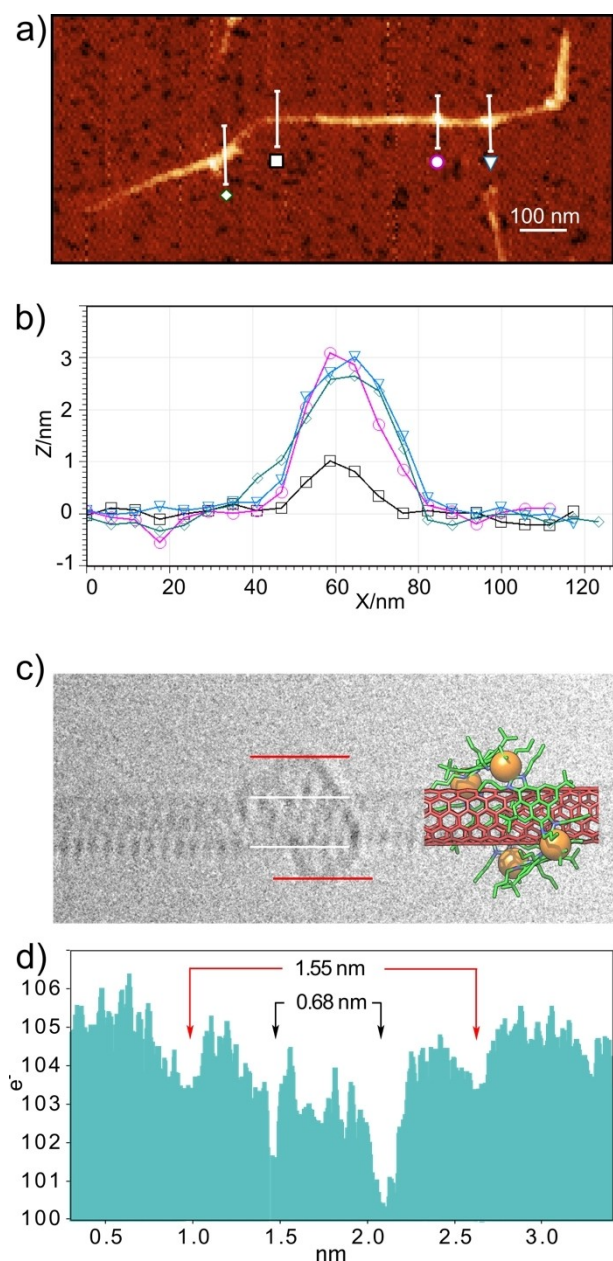
Figure 3. a) AFM topographic image of MINT-**1** as obtained from a dropcast of a suspension in TCE. b) Height profiles along the lines depicted in a). c) ac-HRTEM image of MINT-**1**. An energy-minimized molecular model (molecular mechanics, UFF) of MINT-**1** is super-imposed on the right side to serve as visual reference. d) Profile graph of c), showing the dimensions of the SWNT and the macrocycle, in perfect accordance with expectations. Four darker atoms are visible and tentatively assigned to the Pd centers by comparison with the model.

cannot be obtained. A more structurally informative micrograph, obtained in an image aberration corrected microscope at 60 kV is shown in Figure 3c. An isolated SWNT encapsulated within a macrocycle-shaped organic residue is distinguishable with close to atomic resolution. For the free nanotube, a diameter of 0.68 nm was measured, in perfect accordance with a (6,5)-SWNT. Meanwhile, the macrocycle

addend shows a diameter of 1.55 nm, again in great agreement with the dimensions of metallosquare **1** (Figure 3d). Four individual atomic contrasts are also visible, that can be tentatively assigned to the four Pd corners[24] by comparison with the energy-minimized molecular model superimposed in Figure 3c (see the Supporting Information for more micrographs).

In conclusion, we have introduced a new type of MINT consisting of the threading of a SWNT through the well-defined cavity of a palladium-based supramolecular organometallic complex. The preparation of this metallo-MINT can be performed either by the template-formation of the metallacycles around the surface of the SWNT, or by encapsulating the SWNT into the cavity of the preformed metallacycle. To our knowledge, this is the first time that a metallo-MINT is obtained by interlocking a SWNT, thus exemplifying how metal–ligand binding and the directional control of coordination geometries can be used for the preparation of self-assembly structures beyond the molecular level. We also proved that the incorporation of metal atoms into the structure of the MINT has important implications that affect to the electronic nature of these functionalized nanotubes. In particular, PLE maps suggest that a charge-transfer process occurs from the metallo-square to the nanotubes upon photoexcitation. Interlocked structures based on metal coordination have played a prominent role from the early days of the field,[25] including supramolecular functionalization of SWNTs,[26] and up till now, where some of the most complex structures are synthesized using this kind of interactions.[27] We think that our work opens a new field of opportunities for MINTs. We now intend to extend our strategy for threading other types of metallacycles, and to investigate their potential properties in catalysis.

Conflict of Interest

The authors declare no conflict of interest.

Data Availability Statement

The data that support the findings of this study are available from the corresponding author upon reasonable request.

Angew. Chem. Int. Ed. **2022**, *61*, e202208189 (4 of 5)

© 2022 The Authors. Angewandte Chemie International Edition published by Wiley-VCH GmbH

[1] a) P. Singh, S. Campidelli, S. Giordani, D. Bonifazi, A. Bianco, M. Prato, *Chem. Soc. Rev.* **2009**, *38*, 2214–2230; b) N. Karousis, N. Tagmatarchis, D. Tasis, *Chem. Rev.* **2010**, *110*, 5366–5397.

[2] M. F. L. De Volder, S. H. Tawfick, R. H. Baughman, A. J. Hart, *Science* **2013**, *339*, 535–539.

[3] L. Chio, R. L. Pinals, A. Murali, N. S. Goh, M. P. Landry, *Adv. Funct. Mater.* **2020**, *30*, 1910556.

[4] G. Hills, C. Lau, A. Wright, S. Fuller, M. D. Bishop, T. Srimani, P. Kanhaiya, R. Ho, A. Amer, Y. Stein, D. Murphy, Arvind, A. Chandrakasan, M. M. Shulaker, *Nature* **2019**, *572*, 595–602.

[5] A. de Juan, Y. Pouillon, L. Ruiz-González, A. Torres-Pardo, S. Casado, N. Martín, Á. Rubio, E. M. Pérez, *Angew. Chem. Int. Ed.* **2014**, *53*, 5394–5400; *Angew. Chem.* **2014**, *126*, 5498–5504.

[6] A. de Juan, M. Mar Bernal, E. M. Perez, *ChemPlusChem* **2015**, *80*, 1153–1157.

[7] S. Mena-Hernando, E. M. Perez, *Chem. Soc. Rev.* **2019**, *48*, 5016–5032.

[8] a) A. López-Moreno, E. M. Pérez, *Chem. Commun.* **2015**, *51*, 5421–5424; b) L. de Juan-Fernández, P. W. Münich, A. Puthiyedath, B. Nieto-Ortega, S. Casado, L. Ruiz-González, E. M. Pérez, D. M. Guldi, *Chem. Sci.* **2018**, *9*, 6779–6784; c) S. Leret, Y. Pouillon, S. Casado, C. Navío, Á. Rubio, E. M. Pérez, *Chem. Sci.* **2017**, *8*, 1927–1935; d) E. Martínez-Periñán, A. de Juan, Y. Pouillon, C. Schierl, V. Strauss, N. Martín, Á. Rubio, D. M. Guldi, E. Lorenzo, E. M. Pérez, *Nanoscale* **2016**, *8*, 9254–9264.

[9] A. López-Moreno, B. Nieto-Ortega, M. Moffa, A. de Juan, M. M. Bernal, J. P. Fernández-Blázquez, J. J. Vilatela, D. Pisignano, E. M. Pérez, *ACS Nano* **2016**, *10*, 8012–8018.

[10] a) M. Blanco, B. Nieto-Ortega, A. de Juan, M. Vera-Hidalgo, A. López-Moreno, S. Casado, L. R. González, H. Sawada, J. M. González-Calbet, E. M. Pérez, *Nat. Commun.* **2018**, *9*, 2671; b) D. Wielend, M. Vera-Hidalgo, H. Seelajaroen, N. S. Sariciftci, E. M. Pérez, D. R. Whang, *ACS Appl. Mater. Interfaces* **2020**, *12*, 32615–32621.

[11] S. Moreno-Da Silva, J. I. Martínez, A. Develioglu, B. Nieto-Ortega, L. de Juan-Fernández, L. Ruiz-Gonzalez, A. Picón, S. Oberli, P. J. Alonso, D. Moonshiram, E. M. Pérez, E. Burzurí, *J. Am. Chem. Soc.* **2021**, *143*, 21286–21293.

[12] B. Balakrishna, A. Menon, K. Cao, S. Gsänger, S. B. Beil, J. Villalva, O. Shyshov, O. Martin, A. Hirsch, B. Meyer, U. Kaiser, D. M. Guldi, M. von Delius, *Angew. Chem. Int. Ed.* **2020**, *59*, 18774–18785; *Angew. Chem.* **2020**, *132*, 18933–18945.

[13] R. Chamorro, L. de Juan-Fernández, B. Nieto-Ortega, M. J. Mayoral, S. Casado, L. Ruiz-González, E. M. Pérez, D. González-Rodríguez, *Chem. Sci.* **2018**, *9*, 4176–4184.

[14] K. Miki, K. Saiki, T. Umeyama, J. Baek, T. Noda, H. Imahori, Y. Sato, K. Suenaga, K. Ohe, *Small* **2018**, *14*, 1800720.

[15] A. Pöthig, A. Casini, *Theranostics* **2019**, *9*, 3150–3169.

[16] S. Ibáñez, M. Poyatos, E. Peris, *Acc. Chem. Res.* **2020**, *53*, 1401–1413.

[17] a) V. Martínez-Agramunt, S. Ruiz-Botella, E. Peris, *Chem. Eur. J.* **2017**, *23*, 6675–6681; b) V. Martínez-Agramunt, D. G. Gusev, E. Peris, *Chem. Eur. J.* **2018**, *24*, 14802–14807.

[18] a) V. Martínez-Agramunt, E. Peris, *Chem. Commun.* **2019**, *55*, 14972–14975; b) V. Martínez-Agramunt, T. Eder, H. Darmandeh, G. Guisado-Barrios, E. Peris, *Angew. Chem. Int. Ed.* **2019**, *58*, 5682–5686; *Angew. Chem.* **2019**, *131*, 5738–5742; c) C. Vicent, V. Martinez-Agramunt, V. Gandhi, C. Larriba-Andaluz, D. G. Gusev, E. Peris, *Angew. Chem. Int. Ed.* **2021**, *60*, 15412–15417; *Angew. Chem.* **2021**, *133*, 15540–15545.

[19] D. Canevet, M. Gallego, H. Isla, A. de Juan, E. M. Pérez, N. Martín, *J. Am. Chem. Soc.* **2011**, *133*, 3184–3190.

[20] E. M. Pérez, N. Martín, *Chem. Soc. Rev.* **2015**, *44*, 6425–6433.

[21] a) M. S. Dresselhaus, G. Dresselhaus, R. Saito, A. Jorio, *Phys. Rep.* **2005**, *409*, 47–99; b) A. Jorio, R. Saito, *J. Appl. Phys.* **2021**, *129*, 021102.

[22] M. S. Dresselhaus, A. Jorio, M. Hofmann, G. Dresselhaus, R. Saito, *Nano Lett.* **2010**, *10*, 751–758.

[23] S. T. Skowron, T. W. Chamberlain, J. Biskupek, U. Kaiser, E. Besley, A. N. Khlobystov, *Acc. Chem. Res.* **2017**, *50*, 1797–1807.

[24] K. Cao, T. Zoberbier, J. Biskupek, A. Botos, R. L. McSweeney, A. Kurtoglu, C. T. Stoppiello, A. V. Markevich, E. Besley, T. W. Chamberlain, U. Kaiser, A. N. Khlobystov, *Nat. Commun.* **2018**, *9*, 3382.

[25] M. Fujita, F. Ibukuro, H. Hagihara, K. Ogura, *Nature* **1994**, *367*, 720–723.

[26] S. Chichak Kelly, A. Star, M. V. P. Altoé, J. F. Stoddart, *Small* **2005**, *1*, 452–461..

[27] a) Z. Ashbridge, E. Kreidt, L. Pirvu, F. Schaufelberger, J. H. Stenlid, F. Abild-Pedersen, D. A. Leigh, *Science* **2022**, *375*, 1035–1041; b) Y. Wu, Q.-H. Guo, Y. Qiu, J. A. Weber, R. M. Young, L. Bancroft, Y. Jiao, H. Chen, B. Song, W. Liu, Y. Feng, X. Zhao, X. Li, L. Zhang, X.-Y. Chen, H. Li, M. R. Wasielewski, J. F. Stoddart, *Proc. Natl. Acad. Sci. USA* **2022**, *119*, 2118573119; c) S.-L. Huang, T. S. A. Hor, G.-X. Jin, *Coord. Chem. Rev.* **2017**, *333*, 1–26.